Langmuir

ARTICLE

pubs.acs.org/Langmuir

Control of Ostwald Ripening by Using Surfactants with High Surface Modulus

Slavka Tcholakova,*[,†] Zlatina Mitrinova,[†] Konstantin Golemanov,[†] Nikolai D. Denkov,[†] Martin Vethamuthu,[‡] and K. P. Ananthapadmanabhan[‡]

[†]Department of Chemical Engineering, Faculty of Chemistry, Sofia University, 1 J. Bourchier Avenue, 1164 Sofia, Bulgaria

[‡]Unilever Global Research Center, Trumbull, Connecticut 06611, United States

ABSTRACT: We describe results from systematic measurements of the rate of bubble Ostwald ripening in foams with air volume fraction of 90%. Several surfactant systems, with high and low surface modulus, were used to clarify the effect of the surfactant adsorption layer on the gas permeability across the foam films. In one series of experiments, glycerol was added to the foaming solutions to clarify how changes in the composition of the aqueous phase affect the rate of bubble coarsening. The experimental results are interpreted by a new theoretical model, which allowed us to determine the overall gas permeability of the foam films in the systems studied, and to decompose the film permeability into contributions coming from the surfactant adsorption layers and from the aqueous core of the films. For verification of the theoretical model, the gas permeability determined from the experiments with bulk foams are compared with values, determined in an independent set of measurements with the diminishing bubble method (single bubble attached at large air−water interface) and reasonably good agreement between the results obtained by the two methods is found. The analysis of the experimental data showed that the rate of bubble Ostwald ripening in the studied foams depends on (1) type of used surfactant—surfactants with high surface modulus lead to much slower rate of Ostwald ripening, which is explained by the reduced gas permeability of the adsorption layers in these systems; (2) presence of glycerol which reduces the gas solubility and diffusivity in the aqueous core of the foam film (without affecting the permeability of the adsorption layers), thus also leading to slower Ostwald ripening. Direct measurements showed that the foam films in the studied systems had very similar thicknesses, thus ruling out the possible explanation that the observed differences in the Ostwald ripening are due to different film thicknesses. Experiments with the Langmuir trough were used to demonstrate that the possible differences in the surface tensions of the shrinking and expanding bubbles in a given foam are too small to strongly affect the rate of Ostwald ripening in the specific systems studied here, despite the fact that some of the surfactant solutions have rather high surface modulus. The main reason for the latter observation is that the rate of surface deformation of the coarsening bubbles is extremely low, on the order of 10^{-4} s^{-1}, so that the relaxation of the surface tension (though also slow for the high surface modulus systems) is still able to reduce the surface tension variations down to several mN/m. Thus, we conclude that the main reason for the reduced rate of bubble Ostwald ripening in the systems with high surface modulus is the low solubility and diffusivity of the gas molecules in the respective condensed adsorption layers (which have solid rather than fluid molecular packing).

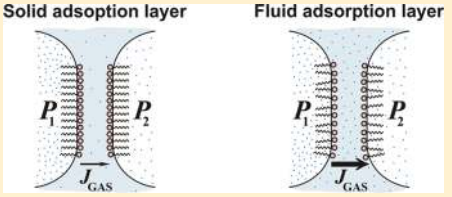

1. INTRODUCTION

The mean bubble size is one of the most important foam characteristics, which determines the foam stability, optical and rheological properties, rate of water drainage, consumer perception for quality, and so forth. Due to the dependence of bubble capillary pressure on bubble size and to the noticeable gas solubility in water (the foam continuous phase), the mean bubble size in foams increases gradually with time, due to gas transfer from the smaller toward the bigger bubbles. This process is known in the literature as "foam coarsening" or "bubble Ostwald ripening" and may be very significant for various foam-based products (e.g., in food and beverage foams).

This process has attracted the attention of practitioners for many years, due to its important practical implications. It is of significant interest from a fundamental viewpoint as well,[1−10] because it involves a complex cascade of gas-transfer processes between the bubbles of various sizes, which is not well understood and still misses univocal theoretical description. Furthermore, the bubble ripening in foams is conceptually related to the particle ripening in several other important systems, such as emulsions, aerosols, precipitates, and alloys, which are also of significant practical and fundamental interest.[11−15]

In the pioneering work of Princen and Mason,[16] a detailed theoretical model was developed which accounted explicitly for the gas diffusion across the surfactant monolayers, covering the foam film surfaces, and across the aqueous core of the foam film, formed in the contact zone between a single bubble and macroscopic air−water interface. On the basis of the proposed model and experiments performed with several surfactant systems, the authors determined the gas permeability of the entire foam films and of the surfactant adsorption layers for several surfactant systems. However, these authors did not try to measure the thickness

Received: October 9, 2011
Revised: November 4, 2011
Published: November 07, 2011

of the foam films, which is an important parameter in the theoretical expression for the film permeability (see, e.g., eq 8 below).

More sophisticated experimental procedure for measuring the film permeability with single bubbles, allowing also for determination of the foam film thickness, was described in ref 17. A large set of experimental results was obtained[17−21] by this method (called "diminishing bubble method") and reviewed recently in ref 22. In these experiments, it was shown that the film permeability depends on various factors, such as electrolyte and surfactant concentrations, temperature, surfactant molecular structure, and so forth. In all these studies,[17−22] the experiments were performed with foam films, formed between single bubbles and the large air−water interface, so that it remained unclear how the experimental results are related to the evolution of the mean bubble size in the actual foams.

In a large number of other experimental[1,4,5,8] and theoretical[1−3,6−8] studies, the major aim was to determine the physical characteristics, controlling the bubble size evolution in coarsening foams. Most of these studies considered two-dimensional (2D) foams for which an analytical expression for the growth rate of the bubbles can be applied (so-called "von Neumann law"). According to the von Neumann law,[23] the rate of change of the size of n-sided bubble is proportional to $(6 - n)$. The theoretical and experimental studies show that the normalized bubble area distribution in such 2D-foams remains invariant during coarsening at longer times and, as a consequence, the average bubble radius varies as $t^{1/2}$ in the long-term regime.[11]

The analysis and the evolution description of the actual 3D-foams are much more complex.[1−3,6−8,24−27] The main theoretical problem arises from the fact that the number of faces of a given bubble depends on the probability distribution of the number of Plateau borders (called "edges" in this literature) per foam film (often called "face"), which is not known in advance and should be either defined theoretically or determined experimentally.[24,25] Numerous theoretical studies[5−8,15,24−28] have been performed to clarify whether the growth rate of individual bubble depends on the bubble topology (number of faces and edges) and what is the exact value of the average number of faces per bubble, f_0, above which the bubbles grow with time (while below f_0 the bubbles shrink). The numerical values of f_0, reported in literature, vary from 13.4 to 15.8.[8,15,28] The theoretical studies and numerical simulations showed[7] that the 3D-foams also reach a long-term scaling regime, in which the average bubble size increases as $t^{0.5}$.

The experimental results for foam coarsening in real 3D-foams are limited[4,8] and most of them are aimed to determine the power-law index for the increase of bubble size with time (especially in the long-term scaling regime). In the experimental study by Durian et al.,[4] the mean bubble size was indeed found to increase as $t^{0.5}$, as predicted theoretically.

The effect of surfactants on the kinetics of foam coarsening was studied experimentally by Saint-Jalmes et al.[29,30] who compared the coarsening in foams stabilized by SDS and Na caseinate. The observed difference in the kinetics of bubble size increase was attributed to the different thicknesses of the foam films, stabilized by these two types of foamers. On the other hand, a number of articles have been recently published in which the bubble coarsening in foams, stabilized by solid particles, was studied. The experiments showed that the solid particles could decrease significantly the rate of bubble coarsening and even can completely arrest it.[31−33] Several mechanisms were proposed in literature for this effect of the solid particles.[31−33]

In our previous study,[34] we found that the addition of fatty acids, as cosurfactants to the surfactant mixture of SLES and CAPB (low-molecular-weight surfactants), leads to significant increase of the dilatational surface modulus of the surfactant solution. This high surface modulus (HSM) was shown to affect significantly the foam-wall viscous friction, the viscous friction inside sheared foams, the rate and mode of foam film thinning, and the rate of bubble Ostwald ripening in the foams.[34] No clear mechanistic explanation was given about the mechanism by which these specific HSM-cosurfactants affect the rate of Ostwald ripening.

The current study is a direct continuation of our previous work, with the major aim being to understand the mechanism by which the HSM-cosurfactants decelerate the Ostwald ripening in these foam systems. The following possibilities are analyzed: the cosurfactants could affect the Ostwald ripening by changing the surface tension of the bubbles (the tension of the shrinking and expanding bubbles being different), the molecular gas permeability of the foam films, and/or the foam film thickness. To achieve our aim, we performed systematic series of experiments with foams, stabilized by several surfactant mixtures with different surface moduli. The performed experiments are analyzed by original theoretical model, which accounts for the overall gas permeability of the foam films, formed between the neighboring bubbles. The values for the film permeability, determined from experiments with foams, are compared with the permeability measured in an independent series of experiments with single bubbles attached to air−water interface. To reveal the mechanism of cosurfactant action, model experiments for determination of the foam film thickness and for characterization of the relevant surface properties of the foaming solutions were performed and analyzed.

The paper is organized as follows: The used materials and methods are described in section 2. The experimental results for the evolution of the bubble size distribution in the studied foams are presented in section 3. The theoretical model for analysis of the experimental results is described in section 4. The verification of model assumptions is presented in section 5. The obtained results for the overall gas permeability in the various systems are presented and discussed in section 6, along with the results obtained from the model experiments with single bubbles. The overall discussion of the results is presented in section 7. The main conclusions are summarized in section 8.

2. MATERIALS AND METHODS

2.1. Materials. As in our previous studies,[34,35] all surfactant solutions contained SLES (product of STEPAN Co., with commercial name STEOL CS-170) and CAPB (cocoamidopropyl betaine, product of Goldschmith, with commercial name Tego Betaine F50) in weight ratio of 2:1. Stock solution of SLES+CAPB (denoted as BS in the text) with total surfactant concentration of 10 wt % was prepared first. Before the actual experiment, this solution was diluted down to 1:20 weight ratio, thus leading to total surfactant concentration in the final foaming solution of 0.5 wt %.

A series of surfactant mixtures was prepared by adding cosurfactants to the SLES+CAPB solution. The following two types of cosurfactants were tested: (1) Cosurfactants ensuring high surface modulus,[34] i.e., lauric acid (LAc), myristic acid (MAc) and lauryl alcohol (LOH); (2) Cosurfactant with low surface modulus, i.e., aminon L-02 Bis-(2-hydroxyethyl)-lauramide (LADA).

The procedure for preparation of the BS+cosurfactant mixture was as follows: First, we prepared the stock solution of SLES+CAPB (BS) with C_{TOT} = 10 wt %. In the so-prepared concentrated solution, we dissolved 1 wt % cosurfactant, under mild stirring and heating, until clear solution was formed. The solution was heated at 60 °C for MAc, and at 45 °C for LAc and LOH, whereas LADA was dissolved without heating. After cooling down to room temperature, the obtained concentrated solution was diluted down to 1:20 weight ratio, with deionized water from Milli-Q water purification system (Millipore). Thus, the surfactant concentration in the final solution was 0.5 wt % BS system + 0.05 wt % cosurfactant.

When the effect of glycerol was studied, the final dilution was made with glycerol−water mixture to reach a final concentration of 40 wt % glycerol.

2.2. Foam Formation and Bubble Size Evolution. The initial foam, containing bubbles with diameter around 0.1−0.2 mm, was prepared by a series of ejection/injection cycles of the foam through a syringe needle, as described in ref 36. Thus-prepared foam was introduced into a Petri dish with height of 3 mm (to avoid significant water drainage in the foam) and covered by an optical prism to avoid evaporation and gas diffusion through the foam−atmosphere interface. The Petri dish was placed in a thermostatted chamber and the temperature was maintained at 20 °C during the experiment.

The bubble size distribution was determined by using the procedure of Garrett et al.[37,38] A video camera, equipped with long-working-distance magnifying lens, was focused on a certain region in the foam sample, which was in contact with the glass prism, and used to capture images of the bubbles for a period of 1 h. The bubble size distribution was determined from these images by using the relation $R_B = (A_{BP}/\pi)^{1/2}$, where A_{BP} is the projected area of a given bubble in contact with the prism wall.[37,38] Image analysis software is used to determine the distribution of the projected bubble areas on the prism wall surface and, hence, of the bubble size distribution in a given moment of the experiment. In this way, we were able to record the evolution of bubble size distribution, as a function of the coarsening time, t. We have checked carefully all samples for bubble coalescence by optical observations. Only systems in which no bubble−bubble coalescence was seen during the entire experiment were included in the paper.

2.3. Bubble under Large Air−Water Interface (Diminishing Bubble Method). By this method, we determined the gas permeability of single foam films, formed between a bubble attached by gravity to an air−water interface.[16,39] A single bubble with an initial diameter of around 400 μm was formed by a syringe needle in a Petri dish, filled with the surfactant solution. The Petri dish was placed in a thermostatted chamber and the temperature was maintained at 20 °C during the experiment. The thermostatted chamber was placed on the stage of microscope Axioplan (Zeiss, Germany), which allowed us to measure precisely the bubble equatorial radius in transmitted light, as well as the radius and thickness of the foam film in reflected light.

The gas pressure inside the bubble is higher than the atmospheric pressure, which leads to permeation of gas across the foam film and to diminishing of the bubble with time. As a consequence, both the bubble radius and the film radius decrease with time. The changes in the bubble size, film radius, and film thickness were measured for a period of several hours. The gas permeability coefficient K was calculated by using the following equation:[39]

$$K = \left[\frac{P_{atm}}{2\sigma}\left(R_0^4 - [R_B(t)]^4\right) + \frac{8}{9}\left(R_0^3 - [R_B(t)]^3\right)\right] / \int_0^t [R_F(t)]^2 \, dt \quad (1)$$

Where P_{atm} is the atmospheric pressure, σ is the surface tension measured by drop shape analysis, R_0 is the initial bubble radius, $R_B(t)$ is the equatorial radius of the bubble at time t, and $R_F(t)$ is the film radius.

2.4. Surface Expansion and Compression of Surfactant Adsorption Layers. Experiments, aimed to determine how large are the deviations of the surface tension from its equilibrium value, upon slow expansion and contraction of the adsorption layer (thus mimicking the surfaces of expanding and shrinking bubbles in coarsening foams), were performed in Langmuir trough model 302LL/D1, Nima Technology Ltd., UK. The area of the adsorption layer was varied with two parallel barriers, which moved symmetrically with a predefined linear speed. The surface pressure was measured by a Wilhelmy plate, made of chromatographic paper. The plate was positioned in the middle between the barriers and oriented in parallel to them. All measurements were performed at 20.0 ± 0.5 °C.

After pouring the surfactant solution into the trough, we waited for the surface tension to reach its equilibrium value. Afterward, the surface area between the two barriers was slowly expanded or compressed, and relatively large surface deformations were applied for a long period of time (1000 s). During this deformation, we could measure the experimental dependence of the surface tension, σ, on the relative surface deformation, α, and on the rate of deformation, $\dot{\alpha}$. From the measured surface tension, we calculated the dependence of the surface stress, τ, on the surface deformation and on the rate of surface deformation

$$\tau(t) = \sigma(t) - \sigma_{EQ} \quad \alpha(t) = \ln\frac{A(t)}{A_0} \quad (2)$$

where $\sigma(t)$ and $A(t)$ are the instantaneous surface tension and layer area, respectively, σ_{EQ} is the equilibrium surface tension, and A_0 is the area of the referent nondeformed state.

3. EXPERIMENTAL RESULTS FOR THE BUBBLE SIZE EVOLUTION IN THE STUDIED FOAMS

3.1. Evolution of the Bubble Size Distribution. The bubble evolution in the studied foams could be described by considering the changes of several characteristics: (1) evolution of the entire bubble size distribution; (2) evolution of the various mean bubble sizes; (3) evolution of the polydispersity of the bubble size distribution. These characteristics are defined below and experimental results are presented to illustrate the main trends.

To account for the fact that the total volume of gas in the system is preserved during the coarsening process, we normalized the bubble size distributions by number and by volume with a factor which arises from the requirement for fixed volume of the system.[40] Thus, the bubble size distribution by number, f_N, is defined as

$$f_N(d_i, t) = \frac{N_i(d_i, t)}{(d_{i+1} - d_i)} \frac{1}{\sum_{i=1}^{N} N_i(d_i, t) d_i^3} \quad (3)$$

where $N_i(d_i, t)$ is the number of bubbles having a diameter in the interval around d_i (from $d_i - \Delta d/2$ to $d_i + \Delta d/2$) per unit volume of the foam, where $\Delta d = d_i - d_{i-1} = d_{i+1} - d_i$ (equal intervals), whereas the sum in the denominator is the volume of all bubbles in the moment t. In a similar way, the bubble size distribution by volume is defined as

$$f_V(d_i, t) = \frac{d_i^3 N_i(d_i, t)}{(d_{i+1} - d_i)} \frac{1}{\sum_{i=1}^{N} N_i(d_i, t) d_i^3} \quad (4)$$

The mean bubble diameters are defined by the following expression:

$$d_{n,n-1} = \sum_{i=1}^{N} N_i d_i^n / \sum_{i=1}^{N} N_i d_i^{n-1} \quad (5)$$

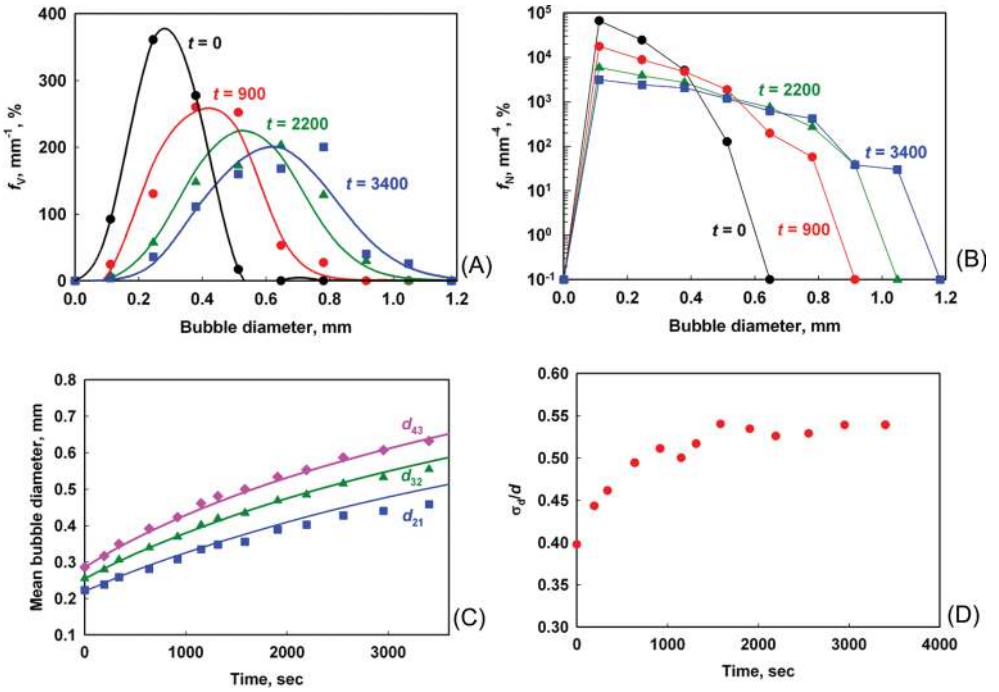

Figure 1. Bubble size distribution by (A) volume and (B) number, after different times as indicated in the figures, for foam stabilized by SLES+Betaine +40 wt % glycerol, $\Phi = 0.9$. (C) Different mean bubble diameters, as a function of time for the same system. (D) Scaled polydispersity as a function of time. The points are experimental data, whereas the curves are theoretical predicted evolution of the mean bubble size by using the theoretical model described in section 4.

For $n = 1$, the above equation defines the mean bubble diameter by number, d_{10}. For $n = 2$, it gives the mean surface-length diameter, d_{21}. For $n = 3$, it defines the mean volume-surface diameter, d_{32}, and for $n = 4$, the diameter d_{43}, which is often called "mean volume diameter", because its value is very close to that of d_{V50} (the actual mean volume diameter).

As a measure of bubble polydispersity we used the normalized value, defined as

$$\frac{\sigma_d}{d} = \frac{\sqrt{\langle (d - \langle d \rangle)^2 \rangle}}{\langle d \rangle} = \sqrt{\frac{d_{21}}{d_{10}} - 1} \qquad (6)$$

where $\langle d \rangle = d_{10}$ is the mean bubble diameter by number.

As an illustration of the evolution of these parameters, we show in Figure 1 the experimental data for foams, stabilized by SLES+Betaine+40 wt % glycerol. One sees that the peak in the distribution by volume is moving with time toward the bigger bubbles, whereas the relative contribution of the small bubbles decreases with time; see Figure 1A. In agreement, the number concentration of the small bubbles, which is given by the product $f_N \Delta d$, decreases significantly with time; see Figure 1B (note that a log-scale is used for f_N). The number concentration of the smallest bubbles decreased more than 20 times during the experiment, which is directly related to the observed increase of the volume and number of the larger bubbles in the foam. This effect is illustrated even better by plotting the mean bubble diameters as functions of time—as seen in Figure 1C, all mean bubble diameters gradually increase with time.

The scaled polydispersity for the same system is presented in Figure 1D as a function of time. One sees that the initial increase of the mean bubble size is accompanied with an increase of the scaled polydispersity; however, in the following period, after 1500 s the scaled polydispersity remains almost constant, $\sigma_d/d = 0.52 \pm 0.02$, which indicates the transition toward the long-term asymptotic behavior. As expected, in this asymptotic regime the mean bubble diameters increase approximately as $t^{1/2}$.

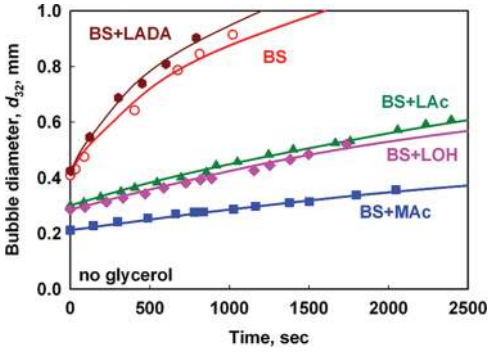

Figure 2. Mean volume-surface diameter, d_{32}, as a function of time, for foams stabilized by BS (empty red circles), BS+LADA (dark red hexagons), BS+LAc (green triangles), BS+LOH (pink diamonds), and BS+MAc (blue squares). All foaming solutions do not contain glycerol and the air volume fraction is $\Phi = 0.9$. The points are experimental data, whereas the curves are theoretically predicted mean bubble size by the model described in section 4.

3.2. Effect of the Studied Factors on the Evolution of the Mean Bubble Diameters. Below, we present experimental results for the various surfactant systems studied, treated as described in section 3.1.

A. Effect of Cosurfactants in the Absence of Glycerol. In this series of experiments, we compared the rate of bubble size increase for foams, stabilized by BS and BS+cosurfactant (LOH, LAc, MAc, or LADA). The obtained results for the mean volume-surface

diameter, d_{32}, are shown in Figure 2. One sees that the increase of d_{32} is significantly faster for foams stabilized by BS and BS+LADA, which have low surface modules (LSM), as compared to the foams stabilized by BS+high surface modulus (HSM) cosurfactants—LOH, LAc, and MAc. The slowest bubble size increase is observed in the foams stabilized by BS+MAc, whereas intermediate rate is measured with LAc and LOH as cosurfactants. From this series of experiments, we can conclude that the cosurfactants ensuring HSM significantly decrease the rate of bubble Ostwald ripening, whereas the cosurfactants with LSM have a relatively small effect. This conclusion was supported with larger set of experiments with other cosurfactants, which are not discussed in the current paper.

B. Effect of Cosurfactants in the Presence of Glycerol. In this series of experiments, 40 wt % glycerol was added to the foaming solutions. The role of the cosurfactants on the mean bubble size in glycerol-containing systems is illustrated in Figure 3, where the evolution of d_{32} for the systems BS, BS+LAc, BS+LOH, and BS+MAc is compared. One sees that the addition of cosurfactants with HSM again leads to reduction of the rate of Ostwald ripening. The lowest rate is observed with foams stabilized by MAc and LOH, whereas LAc has an intermediate effect. However, the relative effect of cosurfactants in the presence of glycerol is less pronounced, compared to the case in the absence of glycerol. This is mainly due to the fact that the addition of 40 wt % glycerol to the foams stabilized by BS leads to significant reduction of the rate of Ostwald ripening (even without cosurfactants); compare Figures 2 and 3. Therefore, we see the combined effects of glycerol and cosurfactants with HSM in the results shown in Figure 3. These two effects are decomposed in the theoretical analysis of the experimental data (see section 6 below).

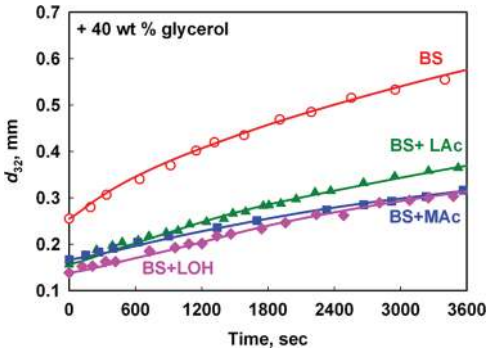

Figure 3. Mean volume-surface diameter, d_{32}, as a function of time, for foams stabilized by BS (red empty circles), BS+LAc (green triangles), BS+LOH (pink diamonds), and BS+MAc (blue squares). All foaming solutions contain 40 wt % glycerol. Air volume fraction is $\Phi = 0.9$. The points are experimental data, whereas the curves are theoretically predicted mean bubble size by the model described in section 4.

4. THEORETICAL MODEL FOR DESCRIPTION OF THE EXPERIMENTAL DATA

The results presented in the previous section clearly demonstrate that both glycerol and HSM-cosurfactants lead to significant deceleration of the Ostwald ripening process. The questions that arise from these results are as follows: (1) what is the reason for the observed effects, and (2) how can we describe quantitatively the experimental data?

The theoretical models described in the literature could be classified into two groups: (1) steady-state mean-field models, which are applicable after a long time only, when a steady-state in the foam evolution is reached, and (2) transient mean-field models which can be used for prediction of the evolution of bubble size distribution, starting from a given initial bubble size distribution.

The first type of model can be used only if the mean bubble size has become much larger than the initial bubble size and the scaled bubble polydispresity has reached a value of ~0.5.[24,25] These types of models are not appropriate for interpretation of our experimental data, because the first requirement is not satisfied; see Figures 1 and 2 above. Therefore, we adapted and modified some of the models from the second group to describe our data.

According to the model developed by Lemlich,[1] the bubbles in the foam could be classified into N classes, each of them having mean bubble size d_i, with the number of bubbles falling into this class being N_i. The change of the moles of gas, n_i, in a bubble with diameter d_i for a period of time, dt, could be expressed by the first law of Fick

$$\frac{dn_i}{dt} = -ks_i\frac{\Delta P}{RT} \quad (7)$$

where n_i presents the moles of gas inside the bubble under consideration, k is the effective permeability (defined per unit area) to the gas transfer across the bubble surface, s_i is the surface area through which the gas transfer occurs, ΔP is the mean pressure difference between the bubble and the other bubbles surrounding it, R is the universal gas constant, and T is the temperature. It is suggested in ref 1 that the pressure difference ΔP could be expressed as the difference between the pressure in the specific bubble under consideration and a hypothetical bubble of some intermediate diameter, ρ, which would be in equilibrium with the mean concentration of gas dissolved in the continuous medium around the bubbles. Furthermore, it was shown rigorously in ref 1 that the diameter of this hypothetical bubble should coincide with the mean surface-length radius, $\rho = r_{21}$, in order to conserve the total volume of gas in the foam during the entire Ostwald ripening process. Lemlich[1] assumed that the area through which the gas transfer takes place, s_i, coincides with the total surface area of the bubble.

The assumptions used in Lemlich's model[1] are justified only for diluted dispersions of separated bubbles or drops, immersed in a liquid medium. However, the bubbles in real foams are compressed against each other, so that thin foam films are formed between them. The thickness of the foam films is much smaller than the thickness of the aqueous layer in the Plateau channels. As a consequence, the transport of gas molecules across the foam films is much faster, as compared to the transport across the Plateau channels, which means that the flux of gas molecules between the neignboring bubbles passes across the foam films exclusively, because the resistance for gas transfer is proportional to the thickness of the liquid layer to be crossed.

Therefore, we modified eq 7 to correspond better to our systems, by substituting the total area of the bubble, s_i, with the total area of the foam films for given bubble, s_{Fi}. In addition, we refined Lemlich's expression for the total gas permeability of the films, k, by introducing the formula of Princen and Mason[16] which accounts for the two distinct contributions—of the gas permeability across the aqueous core of the foam film (with thickness h), and of the gas permeability of the surfactant adsorption monolayers, k_{ml}

$$k = \frac{DH}{h + 2D/k_{ml}} \quad (8)$$

dx.doi.org/10.1021/la203952p |*Langmuir* 2011, 27, 14807–14819

Here, D is the diffusion coefficient and H is the Henry's solubility coefficient of the gas molecules in the liquid phase (viz., in the liquid core of the film).

To calculate the area of the films for a given bubble, we suppose that s_{Fi} is proportional to the total surface area of the bubble, $s_{Fi} \propto s_i = 4\pi r_i^2$, where r_i is the radius of the bubble under consideration. The ratio of the total film area of all bubbles in the foam, S_F, to the total surface area of these bubbles can be expressed by the following equation, proposed by Princen:[41]

$$\frac{S_F}{S_0} \approx \frac{1.083}{\Phi^{2/3}} f(\Phi) \tag{9}$$

where S_0 is the surface area of the nondeformed bubbles, Φ is the air volume fraction, and $f(\Phi)$ is a known function:[41]

$$f(\Phi) = 1 - 3.2/(\Phi/(1-\Phi) + 7.7)^{0.5} \tag{10}$$

Using these assumptions, and taking into account that the driving force of the process is the difference in the gas concentrations in the bubbles of different radii, we modified the approach of Lemlich,[1] and expressed the rate of gas transfer from a bubble, having radius r_i, to the surrounding bubbles as follows:

$$\frac{dn_i}{dt} = -k\frac{S_F}{S_0} s_i \frac{(P_i - P_M)}{RT} \tag{11}$$

where s_i is the area of a nondeformed bubble with radius r_i, P_i is the gas pressure in such bubble, and P_M is the gas pressure in a hypothetical bubble with some intermediate radius that would neither increase not decrease in the given moment, because the average flux of gas toward such bubble would be zero (in average). The value of P_M is defined by eq 18 below. To calculate the pressure inside bubble, P_i, we used an expression derived by Princen[42]

$$P_i = P_{atm} + \frac{\sigma}{r_i}\left(\frac{1-\Phi}{\Phi}\tilde{P}_{OSM}(\Phi) + 2\frac{S}{S_0}\right) \tag{12}$$

where P_{atm} is the atmospheric pressure, σ is the surface tension, and $\tilde{P}_{OSM}(\Phi)$ is the dimensionless osmotic pressure of the foam. Note that eq 12 accounts for both the effect of bubble size and the effect of bubble volume fraction, because the compression of the bubbles in densely populated foam leads to increase of the pressure in the individual bubbles.

For typical polydisperse emulsions, Princen and Kiss[43] found that the following empirical functions describe their experimental data for the osmotic pressure:

$$\tilde{P}_{OSM}(\Phi) = 0.237\left(\frac{\Phi - 0.715}{1-\Phi}\right) - 0.068\ln\left(\frac{0.285}{1-\Phi}\right) - 0.098 \quad 0.715 < \Phi < 0.90 \tag{13a}$$

$$\tilde{P}_{OSM}(\Phi) = \frac{0.00819\Phi^2}{(1-0.9639\Phi)^2} \quad 0.90 < \Phi < 0.99 \tag{13b}$$

In eq 12, S is the total surface area of the deformed bubbles, which can be found[41] by the relation $S/S_0 = 1 + \int_{\Phi_{CR}}^{\Phi}(\tilde{P}_{OSM}/3\Phi^2)\, d\Phi$. Explicit expressions for $S(\Phi)$, corresponding to Princen's functions, are given by eqs 49 and 50 in ref 41. Note that, according to the approach developed by Princen, the dimensionless osmotic pressure of foams and emulsions with the same volume fraction and polydispersity should be the same, because the osmotic pressure is determined only by the surface deformation of the bubbles and drops; therefore, we can apply the same expressions to foams.

Table 1. Film Permeability, k, for Various Systems, as Determined from the Comparison of the Experimental Data for Bulk Foams and the Theoretical Model Described in Section 4[a]

	$k \times 10^5$, m/s	
	no glycerol	+ glycerol
BS	76 ± 25 (75)	16 ± 5 (15.8)
BS+LADA	80 ± 10 (79)	-
BS+LOH	13 ± 4 (12.8)	5 ± 1 (4.9)
BS+LAc	17 ± 5 (16.8)	6 ± 1 (5.9)
BS+MAc	8 ± 1 (7.9)	4 ± 1 (3.9)

[a] The mean values in parentheses are calculated by using eq 14a for dimensionless osmotic pressure, whereas the values without parentheses are calculated by using eq 13b.

For monodisperse foams of equally sized and regularly arranged bubbles, Hoehler et al.[44] proposed the following relation to describe their experimental data for the osmotic pressure:

$$\tilde{P}_{OSM}(\Phi) = 7.3\frac{(\Phi - 0.74)^2}{(1-\Phi)^{1/2}} \quad 0.74 < \Phi < 0.99 \tag{14a}$$

The integration of eq 14a with respect to Φ leads to the following expression for $S(\Phi)$, which corresponds to the function for $\tilde{P}_{OSM}$, introduced by Hoehler et al.:[44]

$$S(\Phi)/S_0 = 1.097 - 2.433(2 + 0.5476/\Phi)\sqrt{1-\Phi} + 5.869\ \mathrm{arctanh}\sqrt{1-\Phi} \quad 0.74 < \Phi < 0.99 \tag{14b}$$

Direct numerical calculations with the expressions proposed by Princen[43] and Hoehler[44] gave very similar results for the film permeability in our systems and lead to the same conclusions; see Table 1 and the discussion in the following section. Therefore, we will not distinguish systematically between these two cases throughout the paper.

Substituting eq 12 into eq 11, we obtain the following expression for the rate of gas transfer from ith bubble to its neighboring bubbles:

$$\frac{dn_i}{dt} = -k\frac{S_F}{S_0} 4\pi r_i^2 \left[\frac{P_{atm}}{RT} + \frac{\sigma}{RT}\left(\frac{1-\Phi}{\Phi}\tilde{P}_{OSM}(\Phi) + 2\frac{S}{S_0}\right)\frac{1}{r_i} - \frac{P_M}{RT}\right] \tag{15}$$

Note that the number of bubbles having radius r_i is denoted by N_i, and each bubble with radius r_i contains n_i moles of gas. Therefore, the total number of moles of gas in the foam is

$$n = \sum_{i=1}^{N} N_i n_i \tag{16}$$

For a closed system, this total amount of gas moles should remain constant during the entire process:

$$\sum_{i=1}^{N}\frac{dN_i n_i}{dt} \approx \sum_{i=1}^{N} N_i \frac{dn_i}{dt} = 0$$

$$-k\frac{S_F}{S_0} 4\pi \sum_{i=1}^{N} N_i r_i^2 \left[\frac{P_{atm}}{RT} + \frac{\sigma}{RT}\left(\frac{1-\Phi}{\Phi}\tilde{P}_{OSM}(\Phi) + 2\frac{S}{S_0}\right)\frac{1}{r_i} - \frac{P_M}{RT}\right] = 0 \tag{17}$$

The term $n_i(dN_i/dt)$ is neglected in the mass balance, eq 17, because the only bubbles that change their number N_i with time are the smallest bubbles, disappearing at the end of their shrinkage. However, these smallest bubbles contain a negligible content of gas, $n_i \rightarrow 0$, so that the product $n_i(dN_i/dt)$ has no contribution to the total mass balance. Thus, we obtain for the mean pressure, P_M

$$P_M = P_{atm} + \frac{\sigma}{r_{21}}\left(\frac{1-\Phi}{\Phi}\tilde{P}_{OSM}(\Phi) + 2\frac{S}{S_0}\right) \quad (18)$$

which is the analogue of the mean effective bubble diameter, ρ, introduced by Lemlich,[1] with an additional account for the effect of air volume fraction on the internal pressure of the bubbles. Introducing this expression for P_M into eq 15, we obtain the following expression for the rate of change of the gas moles in bubble with radius, r_i:

$$\frac{dn_i}{dt} = -k\frac{S_F}{S_0}4\pi r_i^2\frac{\sigma}{RT}\left(\frac{1-\Phi}{\Phi}\tilde{P}_{OSM}(\Phi) + 2\frac{S}{S_0}\right)\left(\frac{1}{r_i}-\frac{1}{r_{21}}\right) \quad (19)$$

On the other hand, following Princen and Mason,[16] we can assume that the gas in the bubbles obeys the ideal gas law:

$$n_i = \frac{P_iV_i}{RT} \quad (20)$$

Therefore

$$\frac{dn_i}{dt} = \frac{P_i}{RT}\frac{dV_i}{dt} + \frac{V_i}{RT}\frac{dP_i}{dt} \approx \frac{P_i}{RT}\frac{dV_i}{dt} \approx \frac{P_{atm}}{RT}\frac{dV_i}{dt} \quad (20a)$$

where we have used the fact that the change of the moles of gas inside the bubble leads mainly to change of the bubble volume (the pressure change is relatively small compared to the atmospheric pressure). Comparing eqs 19 and 20a, we derive

$$\frac{dr_i}{dt} = -k\frac{S_F}{S_0}\frac{\sigma}{P_{atm}}\left(\frac{1-\Phi}{\Phi}\tilde{P}_{OSM}(\Phi) + 2\frac{S}{S_0}\right)\left(\frac{1}{r_i}-\frac{1}{r_{21}}\right)$$
$$= -F(\Phi)\left(\frac{1}{r_i}-\frac{1}{r_{21}}\right) \quad (21)$$

where $F(\Phi)$ depends on the material characteristics of the foam, but does not depend on r and t. Note that $r_{21}(t)$ is also a function of time. Thus, at a given moment, t, the bubbles with size bigger than r_{21} increase their size, whereas the bubbles with size smaller than r_{21} decrease their size, as a result of the Ostwald ripening process.

To proceed further, we use the fact that the bubble size distribution by number $f_N(r,t)$ satisfies the continuity equation along the Ostwald ripening process:[45−48]

$$\frac{\partial f_N(r,t)}{\partial t} + \frac{\partial}{\partial r}(f_N(r,t)\psi(r,t)) = 0 \quad (22)$$

where $\psi(r,t) = dr/dt$ for our system is given by eq 21. To solve numerically the partial differential eq 22, we followed the common practice[40] to reduce it to a set of ordinary differential equations, by discretizing the functions with respect to r. Following the scheme described in ref 40, we divided the bubbles in the system into $N + 1$ classes, starting from 0, r_1, r_2, ..., r_N, where r_N is chosen in such a way that $f(r_{N+1}, t = t_{end}) = 0$ at the end of the process. The discrete intervals $r_2 - r_1 = r_3 - r_2 = ... = r_N - r_{N-1} = \Delta r$ are all equal.

The number of bubbles having radii between r_1 and r_2 (per unit foam volume) is denoted by p_2, whereas the number of bubbles having radii between r_{j-1} and r_j is denoted by p_j. The latter is related to the number distribution, $f_N(r,t)$, by the integral

$$p_j = \int_{r_{j-1}}^{r_j} f_N(r,t)\,dr \quad (23)$$

Using eqs 22−23 and the fact that for sufficiently small intervals

$$f_N(r_j,t) = \frac{p_{j+1}(t) + p_j(t)}{2\Delta r} \quad (24)$$

we derive the following set of ordinary differential equations:

$$\frac{dp_2}{dt} = \frac{p_2(t)}{\Delta r}\frac{dr_1}{dt} - \frac{p_2(t) + p_3(t)}{2\Delta r}\frac{dr_2}{dt}$$
$$\frac{dp_j}{dt} = \frac{p_j(t) + p_{j-1}(t)}{2\Delta r}\frac{dr_{j-1}}{dt} - \frac{p_{j+1}(t) + p_j(t)}{2\Delta r}\frac{dr_j}{dt} \quad j \geq 3 \quad (25)$$

where dr_j/dt are expressed by eq 21. Assuming that the time-step is sufficiently small, we can linearize the above equations to obtain the values of $p_j(t + \delta t)$ from the preceding values $p_j(t)$:

$$p_2(t+\delta t) = p_2(t) + \frac{p_2(t)}{\Delta r}[r_1(t+\delta t) - r_1(t)] - \frac{p_2(t) + p_3(t)}{2\Delta r}[r_2(t+\delta t) - r_2(t)]$$
$$p_j(t+\delta t) = p_j(t) + \frac{p_j(t) + p_{j-1}(t)}{2\Delta r}[r_{j-1}(t+\delta t) - r_{j-1}(t)] - \frac{p_{j+1}(t) + p_j(t)}{2\Delta r}[r_j(t+\delta t) - r_j(t)] \quad j \geq 3 \quad (26)$$

For calculation of $r_j(t + \delta t)$, we solved analytically eq 21, under the reasonable assumption that r_{21} is a constant for the (relatively short) time interval between t and $t + \delta t$. The following expression was derived:

$$F(\Phi)\delta t = r_{21}(t)[r_j(t+\delta t) - r_j(t)] + r_{21}^2(t)\ln\frac{r_j(t+\delta t) - r_{21}(t)}{r_j(t) - r_{21}(t)} \quad (27)$$

From eq 27 we determined $r_j(t + \delta t)$ which is needed to solve eq 26. If the calculated difference $r_j(t + \delta t) - r_j(t)$ is smaller than the predefined value of Δr, we calculated $p_j(t + \delta t)$ and $f(r_j, t + \delta t)$ from eqs 26 and 24, respectively, and determined the new value of the mean bubble radius, $r_{21}(t + \delta t)$. Otherwise, we decreased the time-step and repeated the calculations until the requirement $r_j(t + \delta t) - r_j(t) < \Delta r$ was fulfilled for each class of bubbles, j.

For calculation of $r_{21}(t + \delta t)$, we used

$$r_{21}(t+\delta t) = \frac{\sum_{i=1}^{N} r_i^2(t+\delta t)f_N(r_i, t+\delta t)}{\sum_{i=1}^{N} r_i(t+\delta t)f_N(r_i, t+\delta t)} \quad (28)$$

The value of $r_{21}(t + \delta t)$, determined from eq 28, is used for calculation of $r_{21}(t) = [r_{21}(t + \delta t) + r_{21}(t)]/2$, and with this new value, we calculated again $r_j(t + \delta t)$, $p_j(t + \delta t)$, and $r_{21}(t + \delta t)$. This iterative procedure stops when the difference between the

values of $r_{21}(t + \delta t)$, calculated in two consecutive iterative steps, becomes smaller than 10^{-6} in dimensionless units, because the calculation of the gas fluxes between the bubbles is based on the assumption that r_{21} is constant within an incremental time step in the calculations. The iterative loops used in the numerical scheme, as described above, are schematically represented in Figure 4.

By using this numerical procedure, we can predict the evolution of the bubble size distribution in the foams, if the film permeability, k, and the initial bubble size distribution are known. Since we do not know in advance the film permeability for the studied foams, we used the theoretical model to fit the experimental data for the bubble size evolution with the single adjustable parameter being the film permeability, k. The description of the experimental results with the proposed model is demonstrated in Figures 1′−3, where the points are experimental data, whereas the curves are drawn according to the model. One sees that the description of the experimental results is relatively good, and thus we could determine the values of k for the surfactant systems studied.

5. VERIFICATION OF THE MODEL ASSUMPTIONS

As explained in the previous section, from the best fit to the experimental data for a given surfactant system, we can determine the value of k, which has the meaning of foam film permeability with respect to gas transfer (per unit area of the foam films). The values of k, determined for the various surfactant systems, are compared in Table 1. These values are determined under the following assumptions: (1) The average film thickness between the different bubbles in the foam is constant during the entire period of foam coarsening, and (2) all bubbles in a given foam have the same surface tension. These two important assumptions of the model are checked with independent experiments and some theoretical estimates, described in the current section.

The thickness of the foam films formed from BS and BS+MAc solutions, at two different capillary pressures of 50 Pa (corresponding to mean bubble radius in the foam of ∼1 mm) and 10^4 Pa (corresponding to mean bubble radius of 2 μm) was measured by the capillary cell method.[49,50] At both pressures studied, the film thickness for BS and BS+MAc coincide in the frame of our experimental accuracy—at 50 Pa, the measured film thicknesses were 35 ± 3 nm and 39 ± 3 nm for BS and BS+MAc, respectively. At 10^4 Pa, the measured film thicknesses were 16 ± 3 nm for BS and 14 ± 2 nm for BS+MAc. One sees that, at both pressures, which cover the entire range of bubble diameters of interest in the present study, the thicknesses of the films for BS and BS+MAc differ by less than 15%, whereas the difference in the film permeability is larger than 9 times. Therefore, we can conclude unambiguously that the reason for the different rates of Ostwald ripening in BS and BS+MAc stabilized foams is not related to different film thicknesses in these two systems. Similar film thicknesses were determined with all other foaming solutions studied.

To account for the possible change of the film thickness in a given system, along the coarsening process, due to the increasing bubble size and the related decrease of the bubble capillary pressure, we calculated the dependence of h on the compressing capillary pressure, by taking into account the fact that these films are electrostatically stabilized. For quantitative description of the dependence of the film thickness on the capillary pressure, we

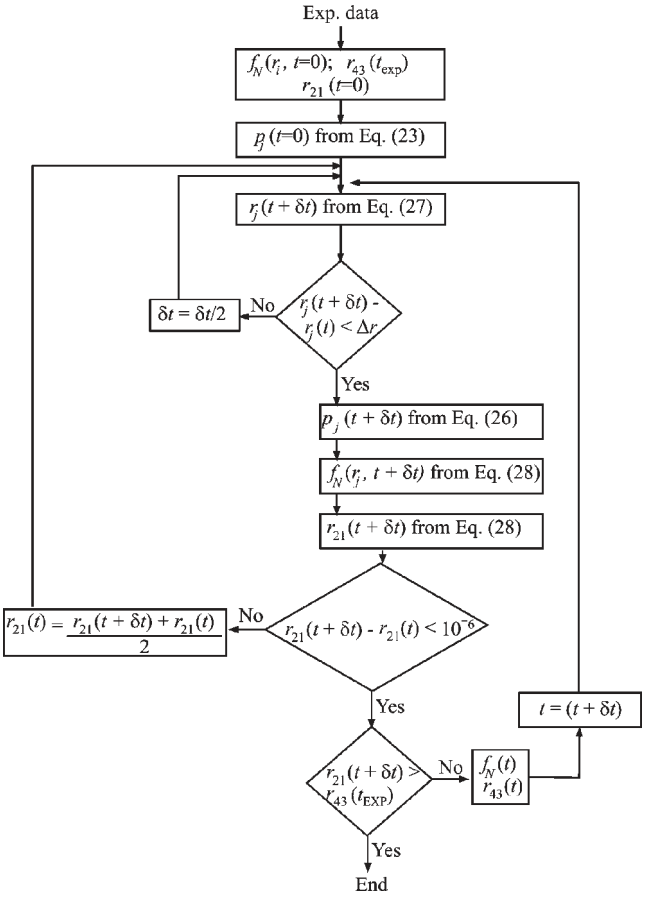

Figure 4. Schematic presentation of the numerical procedure described in section 4.

used the following expression:[50−52]

$$\Pi(h) = 64C_{el}RT\left[\tanh\left(\frac{e\psi_S}{4k_BT}\right)\right]^2 \exp(-\kappa h) - \frac{A_H}{6\pi h^3} \quad (29)$$

where the first term accounts for the electrostatic repulsion and the second term accounts for the van der Waals attraction. In eq 29, C_{el} is electrolyte concentration, R is universal gas constant, T is temperature, e is elementary charge, k_B is Boltzmann constant, ψ_S is surface potential, κ is Debye parameter, A_H is Hamaker constant, and h is the film thickness. For the systems studied, the electrolyte concentration is 7.5 mM, which gives the Debye length of $\kappa^{-1} \approx 3.5$ nm. Assuming $\psi_S \approx 100$ mV[50] and $A_H = 4 \times 10^{-20}$ J,[52] we calculated the $\Pi(h)$ isotherm of the foam films, which predicted that the film thicknesses at 50 Pa and 10^4 Pa are 32 and 16.5 nm, respectively, which is in an excellent agreement with the experimentally determined values of 35 and 16 nm. These estimates support the assumption that the studied films are electrostatically stabilized. Furthermore, using the calculated $\Pi(h)$ isotherm, we can estimate that the film thickness in the actual foams should increase upon coarsening from 26 nm (at 500 Pa for small bubbles) up to 29 nm (at 150 Pa for the larger bubbles). This change of the film thickness is rather small and does not significantly affect the numerical results or the conclusions drawn from the performed study. Therefore, we can conclude from these estimates that the assumption of constant film

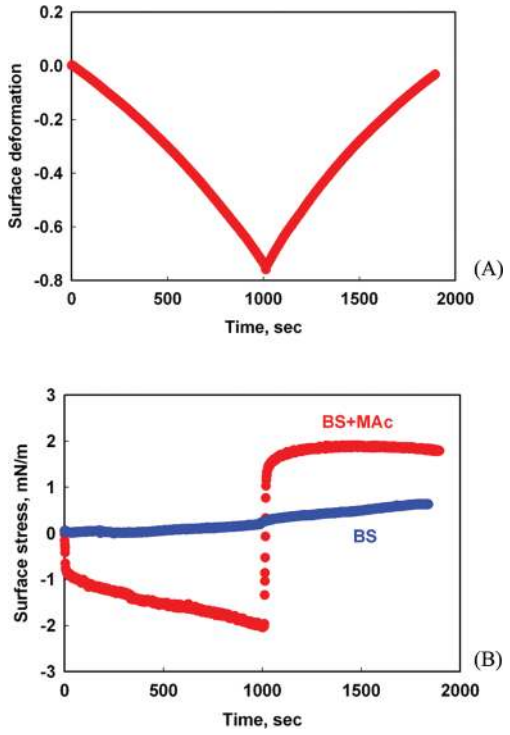

Figure 5. (A) Applied surface deformation and (B) measured surface stress, as functions of time, for adsorption layers formed from 0.5 wt % (SLES+CAPB) + 0.025 wt % MAc (red symbols) and 0.5 wt % (SLES+CAPB) (blue symbols).

thickness along the coarsening process is satisfied with very reasonable accuracy.

A possible explanation for the different gas permeability in the foams stabilized by BS and BS+MAc could be related to the different driving forces (expressed through the bubble capillary pressures) in these two systems. Namely, in our previous studies[34] we showed that BS+MAc solutions have much higher surface dilatational elasticity than BS solutions. This high elasticity suggests that the expanding bubbles may have higher surface tension compared to the shrinking bubbles in a given foam. The different surface tension, in turn, would change the capillary pressures driving the bubble coarsening—an effect which is not included in our model.

Therefore, we measured the dynamic surface tension for slowly expanding and shrinking adsorption layers in Langmuir trough, under conditions resembling those of the bubble surfaces in the coarsening foams. Previous experiments[34] with BS+MAc adsorption layers showed that the surface stress for this system depends on both the surface deformation and the rate of surface deformation. Therefore, we first estimated the typical surface deformation and the rate of surface deformation for the bubbles in the studied foams. The rate of surface deformation was estimated for the largest bubbles in the foam, because they show the highest rate of surface expansion (where the variations in the surface tension are expected to be the biggest), and for BS+MAc system, we found $\dot{\alpha} \approx 5 \times 10^{-4}$ s^{-1}. The maximum surface deformation during the entire foam experiments was ~0.7 for the largest bubbles in the foams. It is very difficult to determine accurately the rate of bubble size decrease for the smallest bubbles in the foam, due to the larger uncertainty in the actual size evolution of these small bubbles. However, the contribution of these small bubbles in the total air volume in the foam is negligible, so we could assume for this estimate that the conditions during the surface shrinking of the small bubbles are similar to those for the expanding large bubbles.

To check how significant the deviations of the surface tension are, upon expansion and shrinking of the bubbles, we performed experiments in the Langmuir trough by the procedure described in section 2.4 above, for values of α and $\dot{\alpha}$ mimicking those in the studied foams. The obtained results for BS and BS+MAc solutions are shown in Figure 5. One sees that the surface stress remains almost zero for the BS solutions, which means that, at the used rate of surface deformation, $\dot{\alpha} \approx 8 \times 10^{-4}$, the adsorption layer in BS-stabilized foams relax rapidly and all bubbles in the foam have the same surface tension. The small drift in the surface tension of this system, observed in Figure 5 after 1000 s, is an artifact of the measurement that does not affect any of the conclusions. On the other hand, the surface stress in BS+MAc decreases steeply during compression and increases rapidly upon expansion, thus creating some difference between the surface tension of compressing and expanding surfaces. However, we found that this difference is relatively small, ~4 mN/m only.

To check whether the detected difference in the surface tension of the shrinking and expanding bubbles in the BS+MAc stabilized foams affect significantly the data interpretation, we modified the equation for the rate of bubble coarsening (eq 21), with the following approximate expression:

$$\frac{r_i\,\mathrm{d}r_i}{\mathrm{d}t} = -k\frac{\sigma_{21}}{P_{\mathrm{atm}}}F_1(\Phi)\left(\frac{\sigma_i}{\sigma_{21}} - \frac{r_i}{r_{21}}\right) \tag{30}$$

Here, σ_{21} is the equilibrium surface tension for the bubbles with size equal to r_{21}, which neither shrink nor expand in the foam, whereas σ_i is the surface tension of the bubbles with size r_i. As a first-level approximation, we assumed that all bubbles with sizes larger than r_{21} have surface tension 2 mN/m higher than the equilibrium (22 mN/m), whereas all bubbles with $r < r_{21}$ were assigned surface tension 2 mN/m lower than the equilibrium value. This modified model was used to describe the experimental data for BS+MAc foams, and the determined value of k was 10% higher than the value determined under the assumption of equal surface tension of all bubbles in the foam. Therefore, although the effect is not negligible, it is much smaller than the other two effects studied here—of the type of surfactant and of the glycerol added to the aqueous phase.

Therefore, we can conclude that the HSM cosurfactants (such as MAc and LAc) are able to change the surface tensions of expanding and shrinking bubbles in foams, but the difference is relatively small (compared to the mean surface tension) for the systems studied in this paper, and it cannot explain the different rates of Ostwald ripening for BS and BS+HSM stabilized foams.

6. COMPARISON OF THE FILM PERMEABILITY DETERMINED IN FOAM EXPERIMENTS AND BY THE BUBBLE DIMINISHING METHOD

The film permeabilities for BS and BS+LADA stabilized films, determined in our experiments (see Table 1), are in good agreement with those reported in literature for common black films, $k \approx 7 \times 10^{-4}$ m/s.[22] The values for BS+HSM-cosurfactants are much lower than the values reported in the literature even for Newtonian black films, for which the film permeability was shown to be about two times lower, $k \approx 4 \times 10^{-4}$ m/s.[22] Therefore, we have measured rather low film permeability for

BS+HSM-surfactants stabilized foams, which is not related to different film thickness or different surface tensions of the expanding and shrinking bubbles, as shown in the previous section.

To check whether the values of k determined by the proposed model agree with the results from an independent experimental method (the bubble diminishing method), we performed additional experiments with the same surfactant solutions, by using the procedure described in section 2.3. To determine more precisely the value of the film permeability by the bubble diminishing method, K, we used the fact that the contact angles of the common black films surrounding meniscus are very small and that, in such systems, the bubble radius and the film radius are interrelated through the effect of gravity:[51]

$$R_F = \sqrt{\frac{4\Delta\rho g}{3\sigma}} R_B^2 \quad (31)$$

Here, R_F is the film radius of the attached bubble, g is the acceleration of gravity, $\Delta\rho$ is the mass density difference between the two phases (air and surfactant solution), σ is the surface tension, and R_B is the bubble radius. By considering that, for submillimeter-sized bubbles, like those used in our experiments, $S_F \approx \pi R_F^2$, and substituting eq 31 in eq 7, we derived the following simple expression for the film permeability:

$$K = -\frac{3P_{atm}}{2\Delta\rho g t} \ln \frac{R_B(t)}{R_B(t=0)} \quad (contact\ angle\ film - meniscus \approx 0) \quad (32)$$

where $R_B(t=0)$ is the initial radius of the bubble. Note that eq 32 predicts linear dependence of $\ln(R_B)$ vs t; see Figure 6 for illustration of results. Therefore, for determination of K we used the best fit to the lines shown in Figure 6. As expected, the bubble is diminished more slowly in BS+MAc and BS+LAc solutions, compared to the BS solution.

The average values of K determined from the bubble diminishing method and k from the foam experiments are compared in Table 2. One sees that the data for BS coincide in the frame of our experimental accuracy, which means that the developed theoretical model for foam coarsening describes very well the data for these foams. The permeabilities for BS+MAc and BS+LAc solutions, obtained from the bubble diminishing method, are 30–50% higher than those determined from the experiments with bulk foams. Before discussing the possible reasons for this difference, we should note that the reproducibility of the data for the HSM systems in the diminishing bubble method was much lower than that for the BS system and those found with bulk foams. Therefore, we think that the most probable explanation for this discrepancy in the measured permeability by the two methods, for the HSM solutions, is the high sensitivity of the formed HSM adsorption layers to the experimental conditions, such as possible heat-driven convections in the underlying surfactant solution, vibrations of the experimental cell due to its contact with the thermostatting device, evaporation from the foam film, surface contaminations, and other possible artifacts which may occur in this method (the experiments with foams have no any of these specific problems). On the basis of the above analysis, and on the much better reproducibility of the data obtained in the foam experiments, we expect that the results for the film permeability, obtained in the foam experiments, are more reliable than those in the diminishing bubble method.

One should note that, in our particular experimental setup, in which the foams are in contact with the solid wall of the prism used to observe the bubbles, we may expect some effect of this solid wall on the measured rate of Ostwald ripening. This effect is mainly due to the missing bubble neighbors, as compared to bulk foams—around 3 out of 12 nearest neighbors would be missing at close packing of monodisperse spheres; see section 4.2.1 in ref 53. Thus, we could estimate approximately that the rate of Ostwald ripening is reduced by around 25%, due to the lower number of neighbors available for gas exchange. There are more subtle effects, such as the specific arrangement of the bubbles close to a smooth solid wall that are difficult to consider rigorously. Because we are not aware of any simple relation that could be used to correct the foam data for the possible wall effects, and because these effects are close to our experimental accuracy, while being much smaller than the effects of the surfactant type and glycerol discussed in this paper, we have not tried to correct the experimental data for the wall effects.

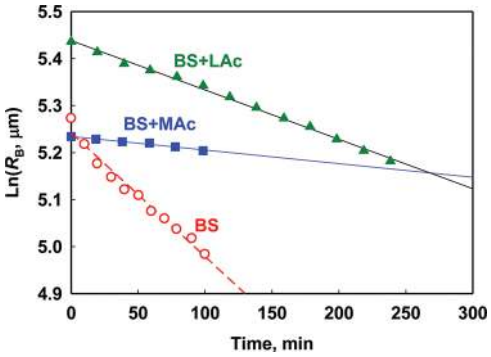

Figure 6. Natural logarithm of bubble radius (measured in μm) as a function of time, as determined by the bubble diminishing method, for bubbles placed in BS+LAc (green circles), BS+MAc (blue squares), and BS (red circles) solutions, respectively.

Table 2. Comparison between the Film Permeability Determined from Experiments with Foams and from Experiment with Diminishing Bubbles Attached to Air–Water Interface

	$k \times 10^5$, m/s	
	foam	bubble under surface
BS	76 ± 25	65 ± 20
BS+LAc	17 ± 5	28 ± 4
BS+MAc	8 ± 2	11 ± 3

7. PERMEABILITY OF THE SURFACTANT ADSORPTION LAYERS

From the experimental results shown in Table 1 and eq 8, we can determine the gas permeability of the surfactant adsorption layers in the systems studied. We assumed that the values of the Henry constant, H, do not depend on the presence of surfactant in the aqueous phase, and took them from literature. Thus, we used in these calculations $H = 0.0199$ (pure water) and $H = 0.008$ in the presence of 40 wt % glycerol.[54] As determined experimentally[16,55] the diffusion coefficients, D, of the nitrogen and oxygen molecules in pure water are very similar, $D \approx 2 \times 10^{-9}$ m^2/s. To account for the effect of glycerol, we assumed that D is inversely proportional to the viscosity of the aqueous phase, which leads to $D = 5.4 \times 10^{-10}$ m^2/s in the presence of 40 wt %

Table 3. Gas Permeability of the Surfactant Monolayers, k_{ML}, and Relative Resistance of the Monolayers (with Respect to the Aqueous Core of the Foam Films), $2D/hk_{ML}$

	$k_{ML} \times 10^3$, m/s		$2D/hk_{ML}$	
	no gly	+ gly	no gly	+ gly
BS	200	250	0.7	0.1
BS+LAc	20	20	7.5	2
BS+LOH	14	13	10	3
BS+MAc	9	10	17	4

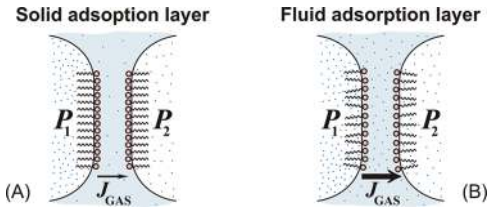

Figure 7. Schematic presentation of the flux of dissolved gas molecules across a foam film stabilized by surfactants with (A) high surface modulus, and (B) low surface modulus. The formation of surface condensed phase of surfactant molecules (by the molecules of myristic acid in the specific surfactant system studied here[34]) leads to very low solubility and diffusivity of the dissolved gas molecules in the condensed adsorption layers on the foam film surfaces. As a result, the gas transfer resistance of the condensed adsorption layers is much higher, as compared to the more common fluid adsorption layers.

glycerol. The film thickness was estimated by eq 29 for all solutions studied. Under these assumptions, we can calculate separately the permeability of the aqueous core of the foam films and of the surfactant adsorption layers for all systems studied; see Table 3. One sees that the permeability of the adsorption layers for HSM-surfactants is much lower than the permeability of the adsorption layers in the BS system. For example, MAc decreases by more than 15 times the permeability of the surfactant adsorption layer. The addition of glycerol does not affect significantly the permeability of the adsorption layers; i.e., the effect of glycerol on Ostwald ripening comes exclusively from the reduced gas solubility and diffusion coefficient in the aqueous core of the film (see eq 8).

The measured gas permeability of the adsorption layers for BS and BS+Gly coincides with the values reported by other authors,[16−21] whereas the layer permeabilities measured with the HSM-containing foams are much lower. Therefore, we can conclude that the main effect of the HSM surfactants is to form condensed adsorption layers on the foam film surfaces which have particularly low gas permeability; see Figure 7. In these systems, the monolayers of long-chain fatty acids are known[34] to pack into the so-called "surface condensed state" which resembles a solid two-dimensional body with different properties, as compared to the more common fluid adsorption layers. The gas solubility and diffusivity in solid bodies is much lower, as compared to fluids, due to the closer packing and lack of mobility of the solidified molecules. The vacancies between the molecules in such solid bodies (which host the dissolved gas molecules) are less and are immobile; therefore, the mechanism of transport of gas molecules in moving vacancies is suppressed in such solid media, in contrast to liquid systems.

From this viewpoint, the studied HSM surfactants stabilize the foams against Ostwald ripening by a different mechanism, as compared to the solid particles. Indeed, the solid particles can decelerate or arrest the Ostwald ripening by jamming the bubble surface, thus affecting strongly the bubble surface tension (see, e.g., refs 31−33), whereas we showed that the surface tension was only slightly affected in the foams studied here.

8. CONCLUSIONS

Systematic measurements of the rate of bubble Ostwald ripening in foams with air volume fraction of 90% are performed, and several surfactants systems are compared which ensure high and low surface dilatational moduli of the foaming solutions. In one series of experiments, glycerol is added to the foaming solutions to clarify how changes in the composition of the aqueous phase affect the rate of bubble coarsening. The experimental results are interpreted by a new theoretical model, which allows us to decompose the overall gas permeability of the foam films into contributions coming from the surfactant adsorption layers and from the aqueous core of the films. For verification of the theoretical model, the gas permeability determined from the experiments with bulk foams are compared with values, determined by the diminishing bubble method, and reasonably good agreement is observed.

The theoretical analysis of the experimental data shows that the rate of bubble Ostwald ripening in the studied foams is strongly affected by two qualitatively different types of factors: (1) Surfactant adsorption layers: surfactants with high surface modulus lead to much slower rate of Ostwald ripening, due to the reduced gas permeability of the adsorption layers in these systems. At a molecular level, the main reason for the observed effect is that the adsorption layers of long-chain fatty acids with high surface modulus are in surface condensed (two-dimensional solid) state. This condensed two-dimensional phase is characterized by low solubility and low diffusivity of the gas molecules inside the closely packed solidified adsorption layers. (2) The presence of glycerol in the aqueous phase (as a substance affecting the solvent properties of water): the glycerol reduces both the gas solubility and gas diffusivity in the aqueous core of the foam film, without affecting the permeability of the adsorption layers, thus also leading to slower Ostwald ripening.

Experiments with a Langmuir trough showed that the possible differences in the surface tensions of the shrinking and expanding bubbles in a given foam are too small to affect strongly the rate of Ostwald ripening in the systems studied here. The reason is that the rate of bubble surface deformation in the foams is rather low, on the order of 10^{-4} s^{-1}, so that even slow relaxation of the surface tension is able to reduce the surface tension variations down to several mN/m.

We should note at the end that, in other systems (e.g., foams stabilized by particles or surfactant−polymer mixtures), other mechanisms for control of bubble Ostwald ripening are possible. For example, the polymer-containing foaming solutions often lead to foam films with thickness up to 200−300 nm, which would lead to lower gas permeability of the film interior, in comparison with the foams studied here. Also, the solid particles are able to jam on the bubble surface, due to their very high barrier to desorption, thus possibly leading to large variations in the surface tension of the bubbles inside given foam. Therefore, the mechanisms discussed in our paper should be considered complementary, rather than competing with the other possible mechanisms

discussed in the literature.[56−60] A similar mechanism, possibly combined with other mechanisms of suppression of Ostwald ripening, should be expected for all surfactants and surfactant mixtures which form condensed adsorption layers on the bubble surface, such as lipids, surfactant + long chain alcohol mixtures, mixtures of cationic and anionic surfactants,[56,58] and so forth.

A specific feature of our study is that we were able, by combining several approaches, to clarify unambiguously the mechanisms involved, as well as the specific contributions of the film interior and of the surfactant adsorption layers into the overall gas permeability of the foam films.

AUTHOR INFORMATION

Corresponding Author

*Phone: (+359-2) 962 5310. Fax: (+359-2) 962 5643. E-mail: SC@LCPE.UNI-SOFIA.BG.

ACKNOWLEDGMENT

The study is funded by Unilever R&D Center in Trumbull, USA. The authors are grateful to Mrs. Radka Petkova for performing the experiments with foam films and to Mrs. Nevena Borisova for performing the experiments with Langmuir trough (both from Sofia University).

REFERENCES

(1) Lemlich, R. Prediction of changes in bubble size distribution due to interbubble gas diffusion in foam. *Ind. Eng. Chem. Fundam.* **1978**, *17*, 89.

(2) Markworth, A. J. Comments on foam stability, Ostwald ripening, and grain growth. *J. Colloid Interface Sci.* **1985**, *107*, 569.

(3) Yao, J. H.; Laradji, M. Dynamics of Ostwald ripening in the presence of surfactants. *Phys. Rev. E* **1993**, *47*, 2695.

(4) Durian, D. J.; Weitz, D. A.; Pine, D. J. Scaling behavior in shaving cream. *Phys. Rev. A* **1991**, *44*, R7902.

(5) Vera, M. U.; Durian, D. J. Enhanced drainage and coarsening in aqueous foams. *Phys. Rev. Lett.* **2002**, *88*, 088304/1.

(6) Hilgenfeldt, S.; Kraynik, A. M.; Koehler, S. A.; Stone, H. A. An accurate von Neumann's law for three-dimensional foams. *Phys. Rev. Lett.* **2001**, *86*, 2685.

(7) Hilgenfeldt, S.; Koehler, S. A.; Stone, H. A. Dynamics of coarsening foams: Accelerated and self-limiting drainage. *Phys. Rev. Lett.* **2001**, *86*, 4704.

(8) Monnereau, C.; Vignes-Adler, M. Dynamics of 3D real foam coarsening. *Phys. Rev. Lett.* **1998**, *80*, 5228.

(9) Vignes-Adler, M.; Weaire, D. New foams: Fresh challenges and opportunities. *Curr. Opin. Colloid Interface Sci.* **2008**, *13*, 141.

(10) Van Der Net, A.; Weaire, D.; Hutzler, S. Rearrangement and elimination of ordered surface layers of crystalline bubble structures due to gas diffusion. *Soft Matter* **2009**, *5*, 318.

(11) Stavans, J. The evolution of cellular structures. *Rep. Prog. Phys.* **1993**, *56*, 733.

(12) Kabalnov, A. S.; Pertzov, A. V.; Shchukin, E. D. Ostwald ripening in emulsions. I. Direct observations of Ostwald ripening in emulsions. *J. Colloid Interface Sci.* **1987**, *118*, 590.

(13) Kabalnov, A. S.; Makarov, K. N.; Pertzov, A. V.; Shchukin, E. D. Ostwald ripening in emulsions. 2. Ostwald ripening in hydrocarbon emulsions: Experimental verification of equation for absolute rates. *J. Colloid Interface Sci.* **1990**, *138*, 98.

(14) Kabalnov, A. S.; Shchukin, E. D. Ostwald ripening theory: applications to fluorocarbon emulsion stability. *Adv. Colloid Interface Sci.* **1992**, *38*, 69.

(15) Glazier, J. A. Grain growth in three dimensions depends on grain topology. *Phys. Rev. Lett.* **1993**, *70*, 2170.

(16) Princen, H. M.; Mason, S. G. The permeability of soap films to gases. *J. Colloid Interface Sci.* **1965**, *20*, 353.

(17) Nedyalkov, M.; Krustev, R.; Kashchiev, D.; Platikanov, D.; Exerowa, D. Permeability of Newtonian black foam films to gas. *Colloid Polym. Sci.* **1988**, *266*, 291.

(18) Nedyalkov, M.; Krustev, R.; Stankova, A.; Platikanov, D. Mechanism of permeation of gas through Newton black films at different temperatures. *Langmuir* **1992**, *8*, 3142.

(19) Krustev, R.; Platikanov, D.; Nedyalkov, M. Permeability of common black foam films to gas. Part 1. *Colloids Surf., A* **1993**, *79*, 129.

(20) Krustev, R.; Platikanov, D.; Nedyalkov, M. Permeability of common black foam films to gas. Part 2. *Colloids Surf., A* **1997**, *123−124*, 383.

(21) Farajzadeh, R.; Krastev, R.; Zitha, P. L. J. Gas permeability of foam films stabilized by an α-olefin sulfonate surfactant. *Langmuir* **2009**, *25*, 2881.

(22) Farajzadeh, R.; Krastev, R.; Zitha, P. L. J. Foam film permeability: Theory and experiment. *Adv. Colloid Interface Sci.* **2008**, *137*, 27.

(23) Von Neumann, J. *Metal interfaces*; American Society for Metals: Cleveland, 1952; pp 108−110.

(24) Jurine, S.; Cox, S.; Graner, F. Dry three-dimensional bubbles: Growth-rate, scaling state and correlations. *Colloids Surf., A* **2005**, *263*, 18.

(25) Thomas, G. L.; De Almeida, R. M. C.; Graner, F. Coarsening of three-dimensional grains in crystals, or bubbles in dry foams, tends towards a universal, statistically scale-invariant regime. *Phys. Rev. E* **2006**, *74*, 021407.

(26) Lambert, J.; Cantat, I.; Delannay, R.; Mokso, R.; Cloetens, P.; Glazier, J. A.; Graner, F. Experimental growth law for bubbles in a moderately "Wet" 3D liquid foam. *Phys. Rev. Lett.* **2007**, *99*, 058304.

(27) Lambert, J.; Mokso, R.; Cantat, I.; Cloetens, P.; Glazier, J. A.; Graner, F.; Delannay, R. Coarsening Foams Robustly Reach a Self-Similar Growth Regime. *Phys. Rev. Lett.* **2010**, *104*, 248304.

(28) Sire, C. Growth laws for 3D soap bubbles. *Phys. Rev. Lett.* **1994**, *72*, 420.

(29) Saint-Jalmes, A.; Peugeot, M.-L.; Ferraz, H.; Langevin, D. Differences between protein and surfactant foams: Microscopic properties, stability and coarsening. *Colloids Surf., A* **2005**, *263*, 219.

(30) Saint-Jalmes, A. Physical chemistry in foam drainage and coarsening. *Soft Matter* **2006**, *2*, 836.

(31) Alargova, R. G.; Warhadpande, D. S.; Paunov, V. N.; Velev, O. D. Foam superstabilization by polymer microrods. *Langmuir* **2004**, *20*, 10371.

(32) Gonzenbach, U. T.; Studart, A. R.; Tervoort, E.; Gauckler, L. J. Stabilization of foams with inorganic colloidal particles. *Langmuir* **2006**, *22*, 10983.

(33) Martinez, A. C.; Rio, E.; Delon, G.; Saint-Jalmes, A.; Langevin, D.; Binks, B. P. On the origin of the remarkable stability of aqueous foams stabilised by nanoparticles: Link with microscopic surface properties. *Soft Matter* **2008**, *4*, 1531.

(34) Golemanov, K.; Denkov, N. D.; Tcholakova, N. D.; Vethamuthu, M.; Lips, A. Surfactant mixtures for control of bubble surface mobility in foam studies. *Langmuir* **2008**, *24*, 9956.

(35) Denkov, N.; Tcholakova, S.; Golemanov, K.; Ananthpadmanabhan, K. P.; Lips, A. Role of surfactant type and bubble surface mobility in foam rheology. *Soft Matter* **2009**, *7*, 3389.

(36) Denkov, N. D.; Subramanian, V.; Gurovich, D.; Lips, A. Wall slip and viscous dissipation in sheared foams: Effect of surface mobility. *Colloids Surf., A* **2005**, *263*, 129.

(37) Garrett, P. R.; Hines, J. D.; Joyce, S. C.; Whittal, P. T. Report prepared for Unilever R&D, Port Sunlight, 1993.

(38) Mukherjee, S.; Wiedersich, H. Morphological and viscoelastic properties of dense foams generated from skin cleansing bars. *Colloids Surf.* **1995**, *95*, 159.

(39) Krustev, R.; Platikanov, D.; Nedyalkov, M. Temperature dependence of gas permeability of Newton black films. *Langmuir* **1996**, *12*, 1688.

(40) Robertson, D.; Pound, G. M. Numerical simulation of heterogeneous nucleation and growth. *J. Cryst. Growth* **1973**, *19*, 269.

(41) Princen, H. M. The structure, mechanics, and rheology of concentrated emulsions and fluid foams. In *Encyclopedia of Emulsion Science and Technology*.; Soblom, J., Ed.; Marcel Dekker: New York, 2001; Chapter 11.
(42) Princen, H. M. Pressure/volume/surface area relationships in foams and highly concentrated emulsions: Role of volume fraction. *Langmuir* **1988**, *4*, 164.
(43) Princen, H. M.; Kiss, A. D. Osmotic pressure of foams and highly concentrated emulsions. 2. Determination from the variation in volume fraction with height in an equilibrated column. *Langmuir* **1987**, *3*, 36.
(44) Höhler, R.; Sang, Y. Y. C.; Lorenceau, E.; Cohen-Addad, S. Osmotic pressure and structures of monodisperse ordered foam. *Langmuir* **2008**, *24*, 418.
(45) Monsalve, A.; Schechter, R. S. The stability of foams: Dependence of observation on the bubble size distribution. *J. Colloid Interface Sci.* **1984**, *97*, 327.
(46) Lialikov, C. S.; Piscounova, V. N.; Chipilov, J. P.; Cerdycev, V. in IXieme Congres Intern. De Photographie Scientifique et Appliquee; Paris, 1935; p 277.
(47) Lifshitz, I. M.; Slyozov, V. V. The kinetics of precipitation from supersaturated solid solutions. *J. Phys. Chem. Solids* **1961**, *19*, 35.
(48) Wagner, C. *Z. Elecktrochem.* **1961**, *65*, 581.
(49) Scheludko, A. Thin liquid films. *Adv. Colloid Interface Sci.* **1967**, *1*, 391.
(50) Kralchevsky, P. A.; Nagayama, K. *Particles at Fluid Interfaces and Membranes: Attachment of Colloid Particles and Proteins to Interfaces and Formation of Two-Dimensional Arrays*; Elsevier: Amsterdam, 2001.
(51) Kralchevsky, P. A.; Danov, K. D.; Denkov, N. D. In *Handbook of surface and colloid chemistry*, Birdi, K. S., Ed.; CRC Press LLS: Boca Raton, 1997; Chapter 11.
(52) Israelachvili, J. N. *Intermolecular and Surface Forces*, 2nd ed.; Academic Press: New York, 1992.
(53) Tcholakova, S; Denkov, N. D.; Ivanov, I. B.; Campbell, B. Coalescence stability of emulsions containing globular milk proteins. *Adv. Colloid Interface Sci.* **2006**, *123*−*126*, 259.
(54) Battino, R.; Rettich, T. R.; Tominaga, T. The solubility of nitrogen and air in liquids. *J. Phys. Chem. Ref. Data* **1984**, *13*, 563.
(55) Ferrell, R T.; Himmelblau, D. M. *J. Chem. Eng. Data* **1967**, *12*, 111.
(56) Varade, D.; Carriere, D.; Arriaga, L. R.; Fameau, A.-L.; Rio, E.; Langevin, D.; Drenckhan, W. On the origin of the stability of foams made from catanionic surfactant mixtures. *Soft Matter* **2011**, *7*, 6557.
(57) Stocco, A.; Rio, E.; Binks, B. P.; Langevin, D. Aqueous foams stabilized solely by particles. *Soft Matter* **2011**, *7*, 1260.
(58) Stocco, A.; Garcia-Moreno, F.; Manke, I.; Banhart, J.; Langevin, D. Particle-stabilised foams: Structure and aging. *Soft Matter* **2011**, *7*, 631.
(59) Stocco, A.; Carriere, D.; Cottat, M.; Langevin, D. Interfacial behavior of catanionic surfactants. *Langmuir* **2010**, *26*, 10663.
(60) Stocco, A.; Drenckhan, W.; Rio, E.; Langevin, D.; Binks, B. P. Particle-stabilised foams: an interfacial study. *Soft Matter* **2009**, *5*, 2215.